A water-immersible two-axis scanning mirror microsystem for ultrasound and photoacoustic microscopic imaging applications

Chih-Hsien Huang, Junjie Yao, Lihong V. Wang, Jun Zou

Chih-Hsien Huang, Junjie Yao, Lihong V. Wang, Jun Zou, "A water-immersible two-axis scanning mirror microsystem for ultrasound and photoacoustic microscopic imaging applications," Proc. SPIE 8616, MOEMS and Miniaturized Systems XII, 861607 (13 March 2013); doi: 10.1117/12.2003087

SPIE.

Event: SPIE MOEMS-MEMS, 2013, San Francisco, California, United States

A Water-Immersible 2-Axis Scanning Mirror Microsystem for Ultrasound and Photoacoustic Microscopic Imaging Applications

Chih-Hsien Huang,[a] Junjie Yao,[b] Lihong V. Wang,[b] and Jun Zou[a]*
[a] Department of Electrical and Computer Engineering, Texas A&M University, College Station, TX 77843, USA; [b] Optical Imaging Laboratory, Department of Biomedical Engineering, Washington University in St. Louis, St. Louis, MO 63130, USA

ABSTRACT

For both ultrasound and photoacoustic microscopic imaging, a fast scanning ability is required, whereas the liquid environment for acoustic propagation limits the usage of traditional MEMS scanning mirrors. In this paper, a new water-immersible scanning mirror microsystem has been designed, fabricated and tested. To achieve reliable underwater scanning, flexible polymer torsion hinges fabricated by laser micromachining were used to support the reflective silicon mirror plate. Two efficient electromagnetic microactuators consisting of compact RF choke inductors and high-strength neodymium magnet disc were constructed to drive the silicon mirror plate around a fast axis and a slow axis, respectively. The performance of the water-immersible scanning mirror microsystem in both air and water were tested using the laser tracing method. For the fast axis, the resonance frequency reached 224 Hz in air and 164 Hz in water, respectively. The scanning angles in air and water under ±10 V AC driving (at the resonance frequencies) were ±13.6° and ±10°. The scanning angles in both air and water under ±16 V DC driving were ±12°. For the slow axis, the resonance frequency reached 55 Hz in air and 38 Hz in water, respectively. The scanning angles in air and water under ±10 V AC driving (at the resonance frequencies) were ±8.5° and ±6°. The scanning angles in both air and water under ±10 V DC driving were ±6.5°. The feasibility of using such a water-immersible scanning mirror microsystem for scanning ultrasound microscopic (SAM) imaging has been demonstrated with a 25-MHz ultrasound pulse/echo system and a target consisting of three optical fibers.

Keywords: scanning mirror, ultrasound image, photoacoustic image

1 INTRODUCTION

Recently, MEMS (microelectromechanical systems) scanning mirrors have been utilized to improve the performances and speed of different high-resolution optical imaging technologies, such as optical coherence tomography [1, 2], confocal microscopy [3] and multi-photon microscopy [4]. Compared with conventional scanning mirrors [5], MEMS scanning mirrors provide some unique benefits such as compact size, low cost, and faster scanning speed. They are especially suitable for developing handheld, endoscopic and even intravascular imaging probes operated inside the human body. Currently, MEMS scanning mirrors are mainly designed for reflecting optical beam in air, which commonly use silicon-based structures and microactuators [5]. However, this feature limits their use for the acoustic imaging technologies such as ultrasound [6] and photoacoustic imaging [7-10], where liquid coupling medium has to be used for acoustic propagation (figure 1). For instance, when working in the water, the brittle silicon supporting structures are vulnerable to the turbulence, shock or unbalanced surface tension force which are often encountered in a liquid environment and may cause to permanent damage. Moreover, excessive cooling, fluidic damping, and electrical shorting could induce significant degradation in the scanning performance (e.g., maximal scanning angle and frequency) or complete device failure. In order to address these issues, we have developed a new water-immersible scanning mirror microsystem, which is capable to operate in both air and water reliably. By utilizing high strength polymer supporting hinges and efficient electromagnetic microactuators, high speed underwater scanning of coaxial optical and ultrasonic beams has been achieved. This novel scanning mirror microsystem can be used in the development of wide-field fast-scanning ultrasonic and photoacoustic microscopic imaging systems.

MOEMS and Miniaturized Systems XII, edited by Wibool Piyawattanametha, Yong-Hwa Park, Proc. of SPIE Vol. 8616, 861607 · © 2013 SPIE
CCC code: 0277-786X/13/$18 · doi: 10.1117/12.2003087

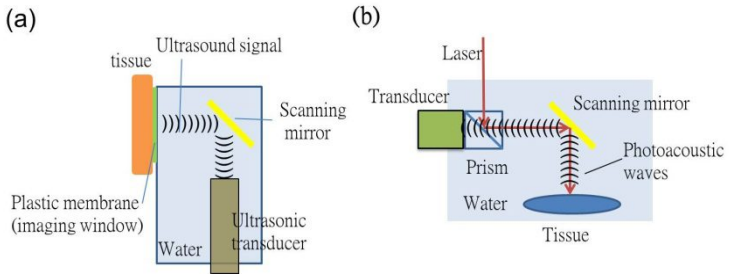

Figure 1. Diagram of micro scanning mirrors operating in the water for (a) pulse-echo ultrasound and (b) photoacoustic microscopic imaging.

2 DESIGN AND FABRICATION

2.1 Design

Fig 2(a) shows the schematic design of the water-immersible scanning mirror, which is composed of a fast-axis module and a slow-axis module. A high-strength BOPET (biaxially oriented polyethylene terephthalate) film is used to make the supporting hinges of the reflective mirror plate in both modules. The high fracture strain and low stiffness of the polymer hinges help to decrease the requirement of driving force and minimize the chance of shock damage [5]. Among all the microactuation mechanisms, including electrostatic, piezoelectric and thermal methods, electromagnetic actuation is chosen as the driving mechanism to enable reliable underwater scanning at low voltage and without thermal effect. As shown in Figure 2(a), compact electromagnetic driving was achieved by combining a single inductor coil and two micro rare-earth magnet discs which are attached underneath the mirror plate with opposite polarities. When current flows through the inductor coil, the interaction between magnetic fields of inductor and permanent magnets create torques on the magnetic discs and thus rotate the mirror plate around the torsional supporting hinges. The entire fast-axis module is attached to the slow-axis module with the support of two BOPET torsional hinges to achieve the second (slow) axis scanning (Figure 2(b) and (c)). To provide the torsional driving force for the slow-axis scanning, four inductor coils and four micro rare-earth magnet discs were arranged into two groups with opposite polarities. Since the mass of slow-axis module is much larger than fast-axis module, the resonant frequency of the slow-axis module is lower. The main benefit of the above modular design is that scanning motion in the two axes is decoupled, which helps to improve the scanning accuracy, linearity and repeatability of both axes.

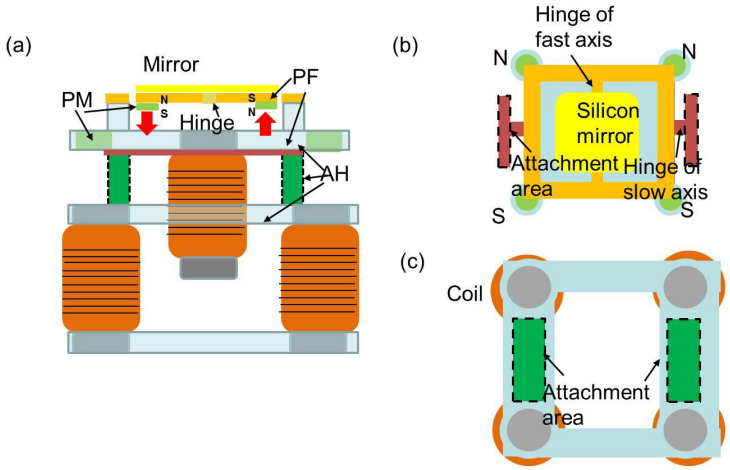

Figure 2. Water-immersible scanning mirror design: (a) side view; (b) top view of fast-axis module; and (c) top view of slow-axis module. AF, actuation force; AH, acrylic holder; PF, polymer frame; PM, permanent magnets.

In both ultrasound and photoacoustic microscopic imaging, the optical and ultrasound signals are typically in the form of short pulses with a repetition rate of kHz. To achieve good quality of resolution with scanning method, the scanning frequency of the fast-axis should be more than 100 Hz and the scanning angle should be larger than 10° to provide a good field of view. The size of the mirror plate should be large enough to reflect acoustic beam completely. Besides, the driving voltages have to be minimized to reduce the complexity of power supply units and decrease the risk of electrical shorting especially in water. The main design parameters of the fast-axis and slow-axis module are listed in Tables 1 and 2.

Table 1. Design parameters of the fast-axis module

Inductor		**Neodymium Magnets**		**Mirror Plate**		**Supporting Hinge**	
Inductance	33mH	**Thickness**	0.8 mm	**Length**	9 mm	**Length**	1 mm
		Diameter	3.125 mm	**Width**	9 mm	**Width**	0.9 mm
				Thickness	500 μm	**Thickness**	75 μm

Table 2. Design parameters of the slow-axis module

Inductor		**Neodymium Magnets**		**Mirror Plate**		**Supporting Hinge**	
Inductance	33mH	**Thickness**	1.6 mm	**Length**	9 mm	**Length**	1 mm
		Diameter	3.125 mm	**Width**	9 mm	**Width**	1.4 mm
				Thickness	500 μm	**Thickness**	75 μm

A preliminary mechanical analysis was conducted based on these design parameters to provide a first-order estimation of their scanning performances (scanning angle, resonant frequency and driving voltage). The magnetic force (F) generated from the interaction of the permanent magnet discs and the inductor coil can be determined by

$$F = V \times Ms \times \frac{\partial H}{\partial z}, \qquad (1)$$

V, Ms, and H are the volume of the permanent magnetic disc, the magnetization of the magnet disc, and the magnetic field intensity generated by inductor. The torque T_{mag} generated by the magnetic force and the resulting rotation angle (ϕ) can be determined by

$$T_{mag} = F \times L', \qquad (2)$$

$$\phi = \frac{TL}{JG}, \qquad (3)$$

where L is the half length of mirror plate, J is torsional moment of inertia, and G is shear modulus of elasticity of the BOPET hinges, respectively and L' is the working length between the magnetic force (F) and the BOPET hinges. For a rectangular cross-section, the torsion moment of inertia (J) can be determined by

$$J = wt^3 \left[\frac{16}{3} - \frac{3.36\,t}{w}\left(1 - \frac{t^4}{12w^4}\right)\right], \qquad (4)$$

In this equation w is the width and t is the thickness of the BOPET hinge. F_{r_air} is the resonant frequency in air of the fast-axis and the slow-axis modules which can be estimated by

$$F_{r\_air} = \frac{1}{2\pi}\sqrt{\frac{K^*}{m}}, \qquad (5)$$

K^* and m are the torsional force DC of the BOPET hinge and the overall effective mass of the fast-axis and the slow-axis modules, respectively. Since the small movement of the mirror plate during scanning and the relatively large mass of the two modules, the damping from the air can be neglected. When the scanning mirror works in water, the resonant frequency (F_{r_water}) can be evaluated by

$$F_{r\_water} = F_{r\_air}\left(\sqrt{1 + \frac{3\pi\rho b}{2\rho m\, t'}}\right)^{-1} \Gamma t\,(\kappa), \qquad (6)$$

where ρ is the density of water, ρ_m is the effective density, and b is the width of the scanning mass. Γ_t (κ) is hydrodynamic functions, and κ is normalized mode numbers [11]. Based on equations (1) to (6), the estimated scanning angles and resonant frequencies of the fast-axis and slow-axis modules are calculated and listed in Table 3.

Table 3. Estimated driving angles and resonance frequencies.

	Fast axis		**Slow axis**
ϕ (DC 16V)	12.8°	**ϕ (DC 10V)**	7.88°
Fr_air	214.38 Hz	**Fr_air**	63.92 Hz
Fr_water	160.06 Hz	**Fr_water**	45.24 Hz

2.2 Fabrication

The fabrication processes of the water-immersible scanning mirror were conducted as follows. First, the reflective mirror plate (9 × 9 mm^2) was diced from a polished single-crystalline silicon substrate. The silicon mirror plate provides not only excellent surface smoothness and flatness, but also good acoustic reflectivity due to the large acoustic impedance mismatch between silicon (19.6×106 N•s/m3) and water (1.47×106 N•s/m3). To improve the optical reflectivity, a thin layer of gold coating (~70 nm thick) was deposited onto the silicon mirror surface using e-beam evaporation. Second, a laser cutting machine are used to fabricate the BOPET torsional hinges and acrylic holders of both fast-axis and slow-axis modules. During the assembly, the silicon mirror plate, the BOPET torsional hinges, the permanent magnet discs (D21B-N52, K&J Magnetics), the inductor coil (70F331AF-RC, BOURNS) and the acrylic holder were attached and bonded together with silicone rubber adhesive (RTV 108, Momentive Performance Materials) to form the fast-axis module. The same procedure was repeated to make the slow-axis module. The fast-axis module was assembled onto the acrylic holder of the slow-axis module (see Figure 2), which was followed by insulating the coils and electrical connections for a reliable underwater operation (Figure 3).

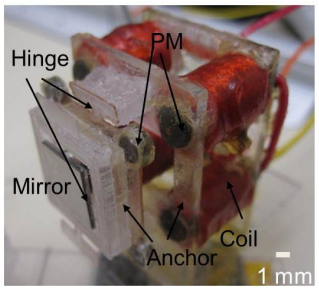

Figure 3. A fully assembled prototype of the water-immersible scanning mirror.

3 CHARACTERIZATION

Laser tracing method was used to measure the scanning angle ϕ and resonance frequency F_r of the scanning mirror in air and water. As shown in Figure 4, the scanning mirror was mounted on the bottom of a water tank. A ruler was placed 6.5 cm away from the center of the mirror plate at an angle of 45°, and a laser beam from a laser pointer was projected onto the mirror plate at an incident angle of 45° and reflected onto the ruler. The scanning angle was calculated based on the moving distance of the laser spot on the ruler. The resonant frequency was determined as the frequency which had maximum scanning angle under the same amplitude of sinusoidal driving voltage. As shown in Figure 4(b), under DC voltage, the scanning angle increased with the driving voltage in both directions (clockwise (CW) and counter clockwise (CCW)). By averaging ten times of measure results, the resulting scanning angle under a 16 V driving voltage was determined as 12°, which matches well with the estimated value. The scanning angles of the fast-axis caused by different driving voltage were similar in air and water. This is because the mirror plate was drive by quasi-static mode and the dynamic damping from water can be negligible. Figure 4(c) indicates that scanning angle increased with the peak driving

voltage in both air and water under sinusoidal voltage driving at the resonance frequency. Since there are larger dynamic damping forces in water than air, the resonance frequency drops from 224 Hz in air to 164 Hz in water, which is similar to the estimation results and the scanning angle under the same driving voltage was decreased.

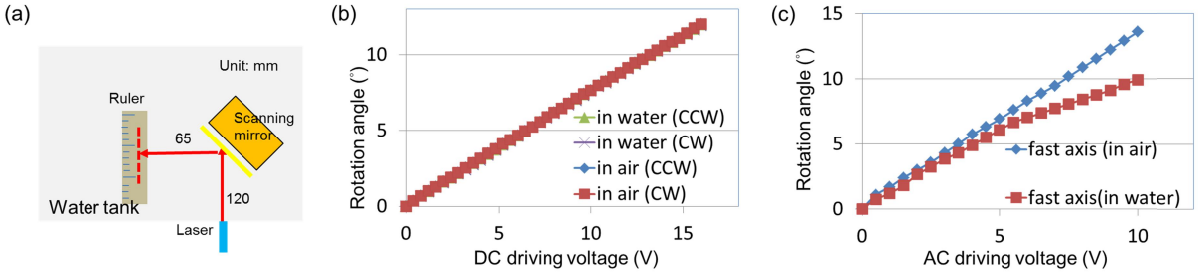

Figure 4. (a) Top view of the characterization setup; (b) Scanning angles of the fast axis with a DC driving voltage; and (c) Scanning angles of the fast axis with an AC voltage at the resonance frequency in air (224 Hz) and water (164 Hz). CW, clockwise; CCW, counter clockwise.

The scanning performance of the slow-axis module was also characterized. As shown in Figure 5(a), under the DC driving condition, the scanning angle achieved 6.5˚ with a 10 V DC driving voltage in both air and water. The resonant frequency was 55 Hz in air and 38 Hz in water. Figure 5(b) shows that with an AC driving voltage of 10 volt (at 55 Hz in air and 38 Hz in water), the scanning angle dropped from 8.5˚ in air to 6˚ in water. Due to the more complex structure of the slow axis module, the estimated rotation angle and resonance frequencies are not accurate as fast axis (which is well described by a lumped parameter model). In addition, a reliability test was done on the fast axis which was driven in water with a AC driving voltage with amplitude of 10V and frequency of 164 Hz for over ten million cycles without noticeable degradation in the scanning performance.

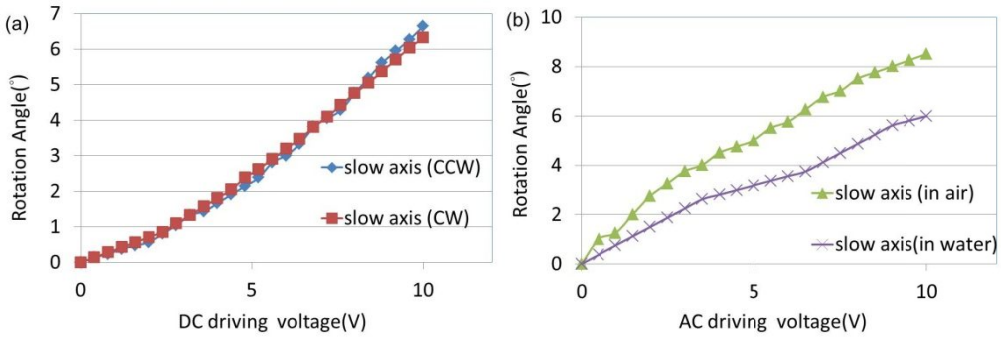

Figure 5. Scanning angles of the slow axis of the water-immersible scanning mirror: (a) With a DC driving voltage; and (b) With a AC voltage at the resonance frequency in air (55 Hz) and water (38Hz). CW, clockwise; CCW, counter clockwise.

4 ULTRASOUND IMAGING EXPERIMENT

The prototype of the water-immersible scanning mirror was used to steer focused ultrasound beam in water to demonstrate the pulse-echo ultrasound microscopic imaging of a optical-fiber target. Figure 6(a) shows the imaging setup which includes a water tank, a high-frequency (25 MHz) focused transducer with a focal length of 19 mm (V324N-SU, Olympus), the water-immersible scanning mirror, and three optical fibers as the imaging target. The scanning mirror was placed 9 mm away from the transducer at an angle of 45˚. The three optical fibers are placed 10 mm away from the center of the mirror plate which are located in the focal zone of the ultrasound transducer to perform a C-Scan microscopic image. The diameter of the optical fibers is 140 μm and the pitches between two adjacent fibers are 0.64 mm and 0.7 mm, respectively. The ultrasound transducer is connected to a pulser/receiver system (5072PR, Olympus) and an oscilloscope (TDX 2014B, Tektronix). The pulses repetition rate and pulse width were set to be 200 Hz and 1 μs, respectively. A DAQ card ((PCI 6251, National Instruments) and a custom-built operational amplifier (LM324N, National Semiconductors) array were used to provide DC voltages to drive the two axes of the scanning mirror. The DC driving voltage of the fast axis was from -10V to 10V with a 0.4V increment

and that of the slow axis was from 0 to 8V with a 0.4V increment. This forms 1000 scanning steps, corresponding to a scanning area of 0.8 mm × 2.6 mm with 20 × 50 pixels. At each "pixel", the received ultrasound signals were measured and averaged 128 times. To automate the scanning and data acquisition process, a LabView (National Instruments) program was developed to control the rotation angle of scanning mirror through DAQ card and recording the signal from oscilloscope. Fig. 6(b) demonstrates the normalized enveloped voltage amplitude in certain time slots as a function of the lateral and vertical scanning location. The distances between the three peaks of the backscattered ultrasound signals were 0.676 mm and 0.728 mm, respectively, which agrees well with the actual distances between the optical fibers.

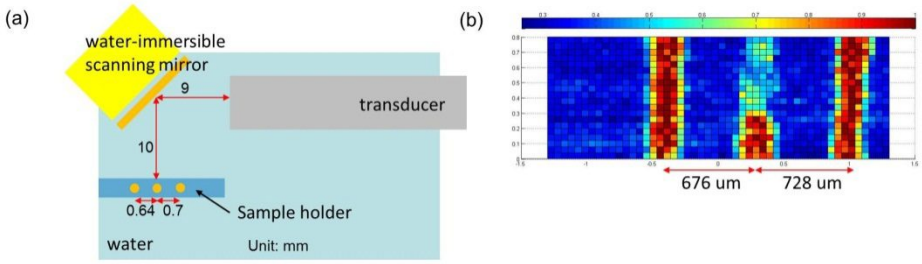

Figure 6. (a) Schematic setup of the pulse/echo ultrasound microscopic imaging setup; and (b) Averaged peak-to-peak voltage of the backscattered ultrasound signal as a function of lateral and vertical scanning location.

CONCLUSION

In conclusion, we have demonstrated a new two-axis scanning mirror microsystem, which is specially designed for reliable and fast underwater scanning of both optical and ultrasonic beams. This unique feature can be potentially used to enhance the imaging capability of scanning acoustic microscopy and photoacoustic microscopy where a liquid matching medium is needed. Future work will focus on the optimization and further miniaturization of the scanning mirror microsystem and also its application in new ultrasound and photoacoustic microscopic imaging modalities.

REFERENCES

[1] Hagelin, P. M., et al., "Scalable optical cross-connect switch using micromachined mirrors," Ieee Photonics Technology Letters. 12(7), 882-884 (2000).
[2] Yang, V. X. D., et al., "Doppler optical coherence tomography with a micro-electro-mechanical membrane mirror for high-speed dynamic focus tracking," Optics Letters. 31(9), 1262-1264 (2006).
[3] Hyejun, R., et al., "Two-dimensional MEMS scanner for dual-axes confocal microscopy," Microelectromechanical Systems, Journal of. 16(4), 969-976 (2007).
[4] Jung, W. Y., et al., "Miniaturized probe based on a microelectromechanical system mirror for multiphoton microscopy," Optics Letters. 33(12), 1324-1326 (2008).
[5] Liu, C., [Foundations of MEMS]. Upper Saddle River, NJ: Pearson/Prentice Hall, 83-94(2006).
[6] Chen, W. H., et al. "Development of sector scanning ultrasonic backscatter microscope." Ultrasonics Symposium, 2000 IEEE. 1681-1684(2000).
[7]Wang, L. V., "Multiscale photoacoustic microscopy and computed tomography," Nature Photonics. 3(9), 503-509 (2009).
[8] Yao, J. and Wang, L. V., "Photoacoustic tomography: fundamentals, advances and prospects," Contrast Media Mol Imaging. 6(5), 332-45 (2011).
[9] Yao, J., et al., "Label-free oxygen-metabolic photoacoustic microscopy in vivo," Journal of Biomedical Optics. 16(7), 076003 (2011).
[10] Wang, L., et al., "Fast voice-coil scanning optical-resolution photoacoustic microscopy," Opt Lett. 36(2), 139-41 (2011).
[11] Cornelis A. V. E., et al.," Resonant frequencies of a rectangular cantilever beam immersed in a fluid," J. Appl. Phys 100(8), 114916 (2006)